Article:
Wang, R, Li, Z, Shi, J et al. (6 more authors) (2021) Color 3D printing of pulped yam utilizing a natural pH sensitive pigment. Additive Manufacturing, 46. 102062. ISSN 2214-7810

https://doi.org/10.1016/j.addma.2021.102062

Color 3D printing of pulped Yam utilizing a natural pH sensitive pigment

Ruiyuan Wang[1a], Zhihua Li[1a,b], Jiyong Shi[a], Melvin Holmes[c], Xinyu Wang[a], Junjun Zhang[a], Xiaodong Zhai[a], Xiaowei Huang*[a], Xiaobo Zou*[a]

[a] School of Food and Biological Engineering, Jiangsu University, Zhenjiang 212013, China

[b] Luzhou Laojiao Co., Ltd.

[c] School of Food Science and Nutrition, University of Leeds, Leeds LS2 9JT, United Kingdom

Tel: +86 511 88780085; Fax: +86 511 88780201

Email address: huangxiaowei@ujs.edu.cn (Xiaowei Huang), zou_xiaobo@ujs.edu.cn (Xiaobo Zou)

[1] These authors contributed equally to this work

* Corresponding author:

Abstract

A novel color control strategy for 3D printing was proposed based on a single channel nozzle with a single raw material. The basic principle was to regulate the pH of the extruded line through electrolysis which would result in the color change of pH-sensitive pigments mixed in the printed materials. Using pulped yam as a feedstock and a pH sensitive pigment extracted from purple sweet potato (PPP), the process parameters were optimized using a moisture content of 35% and a PPP content of 5 mg/100g. Printing tests showed that the color of the extruded line could be conveniently controlled by adjusting the applied electrode potential from -45 to 45 V with a hue range of 0.192-0.916, which exhibited a gradually changing color scheme from mauve to yellow. The proposed strategy showed promising potential in color 3D printing with the advantages of low cost, convenient control and simple composition.

Keywords

Color 3D printing; Electrolysis; Pulped yam; Pigment

1. Introduction

Three-dimensional (3D) printing is a developing technology for generating complex structured objects based on layer-by-layer stacking and deposition [1], [2]. The 3D printing of food has shown great market potential in the food industry for its advantages in flexible customization according to personal preferences [3], [4].

As a novel food manufacturing technology, many meaningful works have been reported to explore the 3D printing of food. Liu, et al. established a milk protein based food simulant for 3D printing and investigated the effect of whey protein isolate concentration on the printing performance of the food simulant [5]. Yang, et al. successfully developed a new 3D printing food construct based on a lemon juice gel system [6]. Yet, to the best of our knowledge, few studies in the field of food 3D printing focused on providing a range of colors for 3D printed products.

To achieve the printing of colored 3D models, continuing efforts have been made to develop novel processes, devices and materials [7], [8]. Indeed, some commercial systems have attained dimensional resolution in the 16 μm range with increasing color saturation in recent years [9]. Despite these successes, the colorization materials and processes are similar having a basis in the general subtractive color theory [10]. This restriction implies that the color change of the materials relies on highly precise fusion or combination of three (Red, Green, Blue) or four (Cyan, Magenta, Yellow and Black) primary colors. However, the precise quantitative control of multiple primary materials would require costly complex mechanical and software design. In addition, the primary

color strategy would also depend on the properties of the primary materials which significantly limits the scope and application of the developed systems. Multi-material or multi-color printing is also a color printing method. Multi-material machines are often equipped with dual extruders or more, which require more complex structure and compact layout [11], [12], [13], [14], [15]. To solve these problems, a more reasonable color control strategy is needed.

Anthocyanins are a group of non-toxic and edible pigments, which change their colors according to pH values [16]. They can present a relatively wide color range due to the molecule structure transformation induced by different pH environments [17]. Anthocyanins exhibit advantages having a wide range of low cost material sources primarily as they present in the vacuoles of flowers, fruits, vascular plants and many other plant tissues [18]. In recent years, anthocyanins have been widely used as colorants in candies, beverages, jams, and dairy products [19], [20], [21], [22]. Therefore, anthocyanins may provide a convenient solution to control the color of printed materials by controlled adjustment of pH.

In terms of pH, the electrolysis method is an effective technique to adjust the pH of materials containing water [23], [24], [25], [26]. Wu, et al. reported that electrolysis can change the pH of a hydrogel resulting in a color reaction of phenolphthalein in the hydrogel [27]. Zhai, et al. reported the use of electrochemical writing to print patterns on polysaccharide films based on the color change of anthocyanins [28]. Therefore, the combination of pH sensitive pigments and electrolysis technique can provide a novel

method for the control of colored 3D printing.

In this study, a single-step color control strategy for 3D printing was proposed by combining pH sensitive pigments with electrolysis technique. Pulped yam (PY) was used as feedstock and anthocyanin extracted from purple sweet potato (Ipomoea batatas L.) was used as the pH sensitive pigment. A special electrolysis nozzle was designed to control the pH value of the extruded yam in real-time which consequently provided a range of desired colors. The proposed strategy showed promising potential in color 3D printing with the advantages of low cost, convenient control and simple structure.

2. Materials and methods

2.1 Materials

Purple sweet potato powder, mulberry powder, carrot powder, black wolfberry powder, roselle powder were obtained from Lvshuai Food Co., Ltd.(Taizhou, China). Iron Stick Yam was obtained from local supermarket. Sodium sulfate was purchased from Sinopharm Chemical Reagent Co., Ltd. (Shanghai, China). All chemicals were of analytical grade and used without any purification.

2.2 Device and process parameters for 3D printing

A 3D food printer from Foodini (Natural Machines, Spain) was modified in hardware and software to achieve the color printing (Fig. 1A). The extruder is configured with a nozzle and a waste channel that unnecessary color-changing materials could be discharged. Platinum wire and nozzle configurations were fabricated as electrodes to realize electrolysis during material extrusion (Fig. 1B). Electrode potential

was applied using a programmable DC power supply (2280S-60-3, Keithley). The color printing process was controlled with a self-developed plugin based on Octoprint system (https://octoprint.org/). The printing was performed with the following parameters according to pre-experiment: layer height of 1.4 mm, nozzle diameter of 1.5 mm, line width of 1.5 mm, extrusion rate of 3.5 mm^3/s.

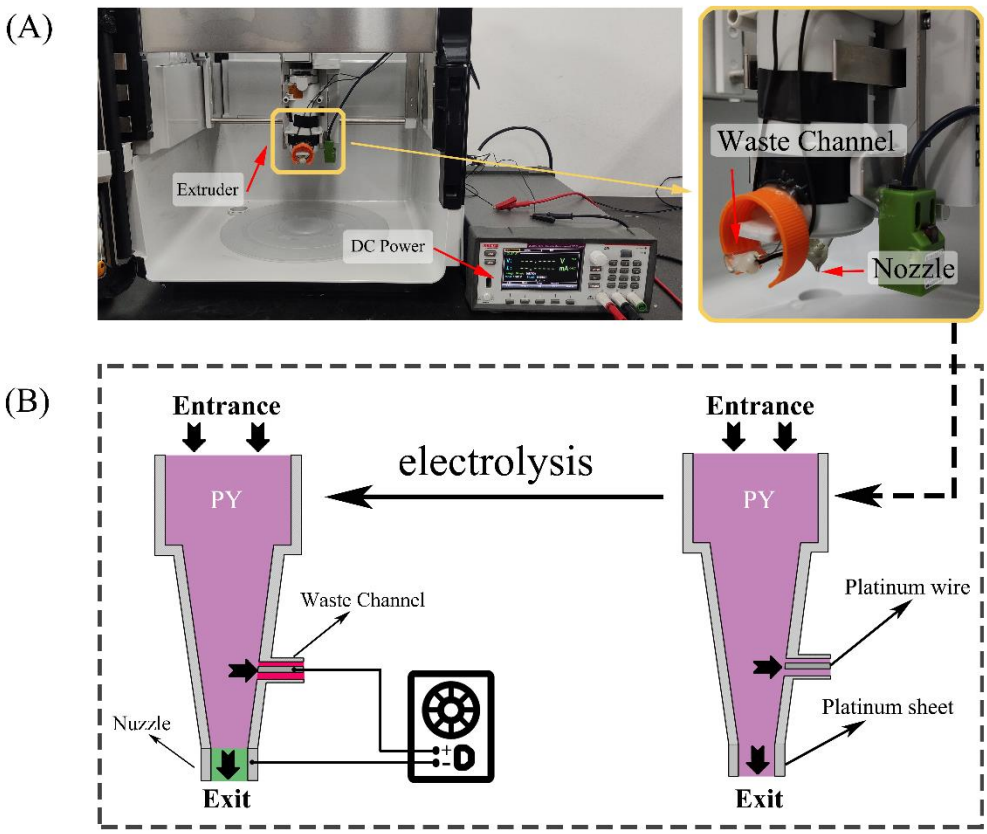

Fig. 1. Images of the color 3D printing device (A) and diagram of the nozzle configuration (B)

2.3 Preparation and characterization of pigments

The pigments utilized for screening were extracted from the powder of purple potato, carrot, mulberry, black wolfberry, roselle [29]. Briefly, 100 g of powder was added into 1 L of 40% (v/v) ethanol, stirred continuously at 60 °C for 12 h in dark

conditions. Then the extracted solution was filtered, concentrated by evaporation on a rotary evaporator at 50 °C also under dark conditions. The concentrated extract solutions were stored at -40 °C for 24 h and then freeze dried.

The color images of purple potato pigment (PPP), carrot pigment (CP), black wolfberry pigment (BWP), mulberry pigment (MP) and roselle pigment (RP) were recorded with pH value varying from 3 to 9 with gradient of 0.2. The H value from the HSV model of the images were extracted to quantitatively represent the color range of the pigments. The spectra from 450 to 760 nm of the pigments were also obtained using an UV–Vis spectrophotometer (Agilent CPRY 100, Varian Corporation, USA).

2.4 Preparation of pulped yam (PY) for printing

Yam was peeled, washed and steamed for 45 minutes, then mixed with water, pigments and electrolytes, stirred for 5 min. Water contents of 25%, 30%, 35%, 40%, 45%, 50%, 55%, 60%, 65%, 70% were screened to optimize the water addition. Pigments contents of 0.5-6 mg/100g (based on the weight of PY, each gradient of 0.5) added to the PY were compared to obtain the appropriate pigments contents. 0.5% of sodium sulfate was mixed in PY as an electrolyte to enhance the electrical conductivity.

2.5 Printability of PY

2.5.1 Rheological measurement

Rheological characterization was carried out by a rotary rheometer (Discovery HR-1, TA Instruments, USA) using a parallel plate attachment (20 mm diameter and 1000 μm gap) according to the method of Liu with slight modification [30]. The PY

sample to be measured was loaded into the plate and equilibrated for 3 min before testing. Then, flow sweep tests were conducted at shear rate range of 0.01–1 s^{-1} and dynamic oscillation frequency analysis was performed at an angular frequency range of 1 to 100 rad/s in the linear viscoelastic region. The storage modulus (G'), the loss modulus (G'') and tan δ (G''/G') were recorded. All tests were performed at 25℃.

2.5.2 Stability measurement

Stability measurements were executed based on the methods of Zhu [31]. A hollow square column (bottom dimension of 20 x 20 mm, wall thickness of 3 mm, shown in Fig. S1) was designed to evaluate the printability of samples. Successive layers of printing continued up to the height until the square column structure collapsed indicating the yield point of the construct. Stability measurements were made three times for each sample.

3. Results and discussion

3.1 Screening of pigments

Five types of natural pigments extracted from purple potato (PPP), carrot (CP), black wolfberry (BWP), mulberry (MP) and roselle (RP) were screened to obtain a wide color range. Fig. 2A shows the images of the PPP, CP, BWP, MP, RP solutions at different pH values (pH 3.0-9.0) with concentration of 10 mg/L, and the corresponding H value is plotted in Fig. 2B. As shown in Fig. 2, PPP and RP exhibited a monotonically decreasing trend with a wider range of H value, indicating a wider color range, compared with other pigments. However, the RP presented a sharp drop in the H value when the pH increased from 4.0 to 4.8 and quite low saturation after the pH was higher than 7.2, which would require high precision of pH control and cause poor tinctorial

power. For PPP, its color changed from red to green with pH increasing from 3.0 to 9.0, corresponding to a continuously and progressively decreased H value. The results agreed well with the reports by Choi, et al., which indicated that PPP had promising potential as a pH sensitive pigment [32]. Therefore, the PPP was selected as the optimal pH sensitive pigment for further development.

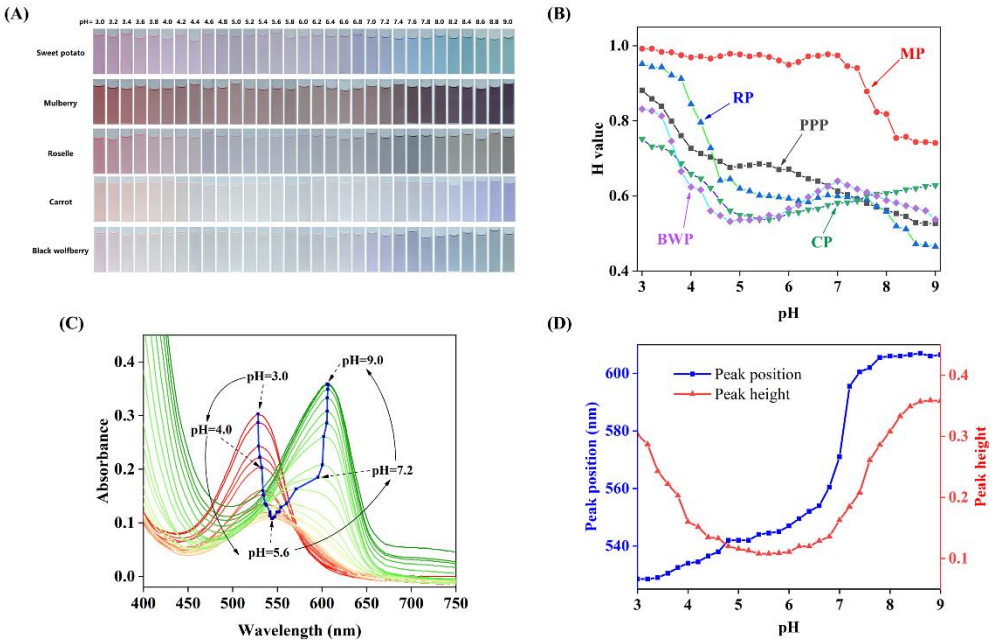

Fig. 2. Color change (A) and corresponding H value (B) of pigments from different plants at pH 3-9; The UV-Vis spectra of purple potato pigment (C) and the corresponding peak changes(D).

The UV-Vis spectra of PPP from pH 3.0 to 9.0 are shown in Fig. 2C. Corresponding with the color changes in PPP solutions, the absorption peak shifted from 528 to 600 nm when the pH increased from 3.0 to 9.0. It was found that the peak wavelength kept increasing, while the peak height decreased first and then increased with pH (Fig. 2D), meaning that the red color of the PPP solution gradually faded, turned to green and gradually deepened. The changing of the spectra agreed well with

the H value, which could be attributed to the structure change of anthocyanin molecules [33]. The anthocyanins mainly presented in the form of flavylium cation within pH 2-3, appearing red. When pH increased to 4.0–6.0, the structures gradually transformed into quinones, transforming to purple. As the pH continued to increase (pH 6-8), a pseudo-base structure was generated and the solution finally turned blue.

3.2 Rheological behaviors of PY

To acquire better printability, the viscosity curve of PY with different moisture content was compared in Fig. 3A. The viscosity of PY decreased significantly with the increase of shear rate, indicating that PY was a typical pseudoplastic fluid exhibiting shear thinning behavior [34], [35], [36]. This behavior could be explained by the gradual orientation of the soluble starch molecules and the breaking of the hydrogen bonds between the amylose molecules [37]. Furthermore, the increase in moisture content led to an overall decrease in viscosity which would facilitate the pass of PY through the nozzle. However, high moisture content would affect the shape retention of the material.

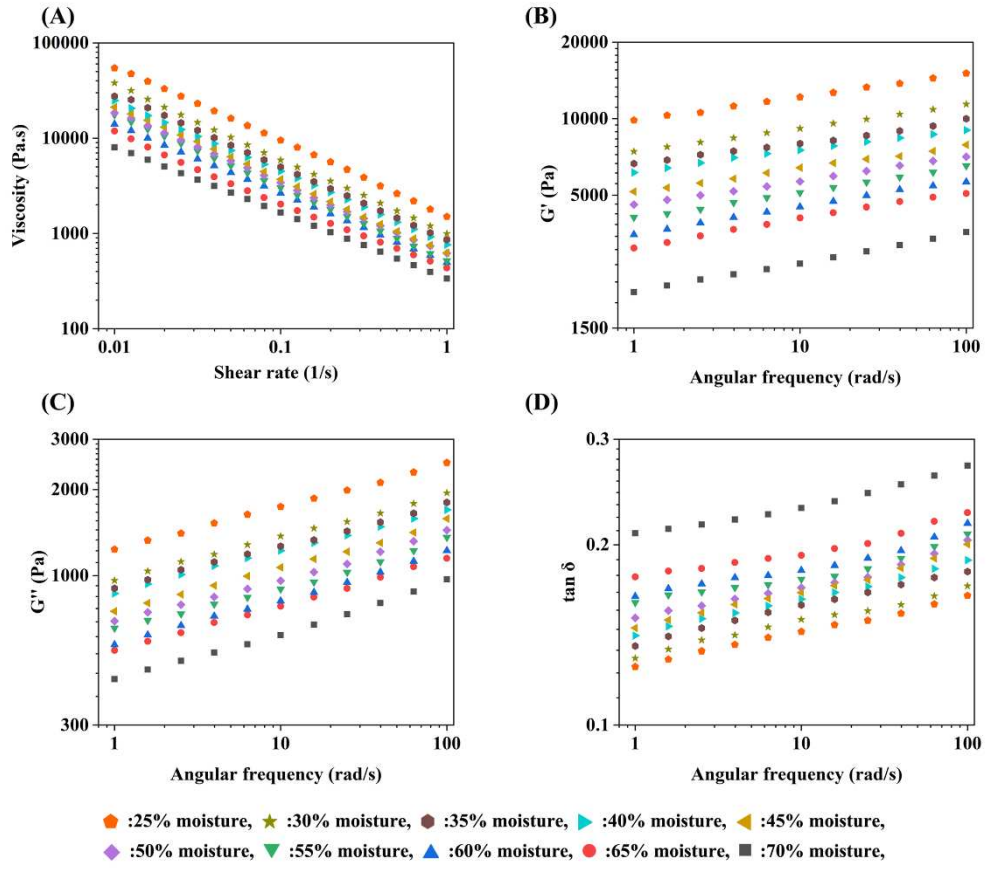

177

178 Fig. 3. The effects of different moisture content of PY on shear rate and viscosity (A), storage

179 modulus (G') (B), loss modulus (G'') (C), tan δ(D).

180 Fig. 3B and Fig. 3C showed the storage modulus (G') and loss modulus (G'') of

181 PY with different moisture content. Both G' and G" increased as the oscillation

182 frequency increased, and G' was higher than G'' at the same moisture content,

183 indicating solid-like properties. Therefore, the PY would have sufficient strength to be

184 stably deposited on the next layer after extrusion through the nozzle [38]. In addition,

185 the increase of moisture induced a simultaneous decline of G' and G'', but resulted in a

186 significant increase of the dynamic mechanical loss tangent (tan δ) calculated as G''/G'

187 (Fig. 3D). The increase of tan δ indicated the decreased ability of energy absorption and

188 lower viscosity which was consistent with the measured viscosity results. This could be

189 explained from the perspective of starch gelatinization [39]. As the water content
190 increased, more water molecules entered the yam starch granules to expand the starch
191 granules resulting in the break of hydrogen bonds between the starch chains.

192 To evaluate the printing performance of PY with different moisture content, the
193 maximum printing height of a hollow square column was measured and presented in
194 Fig. 4. When the moisture content was below 25%, the high viscosity made it very
195 difficult for material extrusion and the extruded line was too dry for the extruded layers
196 to adhere to each other. Therefore, the maximum height of PY samples with moisture
197 content lower than 25% was recorded as 0 directly. With the increase of moisture
198 content from 30% to 70%, the height of the square column gradually decreased. In
199 particular, the wall around the square column softened significantly when the moisture
200 content exceeded 60%, thus no structure could be formed. Unlike the case of high
201 moisture content, the collapse with moisture content between 40% to 60% was mainly
202 caused by the force imbalance of the square column, the structure deviated in one
203 direction and eventually collapsed. As seen from Fig. 4, the sample with moisture
204 content of 35% showed the best printability with a maximum height of 90 mm and
205 exhibited a smoother surface texture. Therefore, 35% was selected as the optimal
206 moisture content.

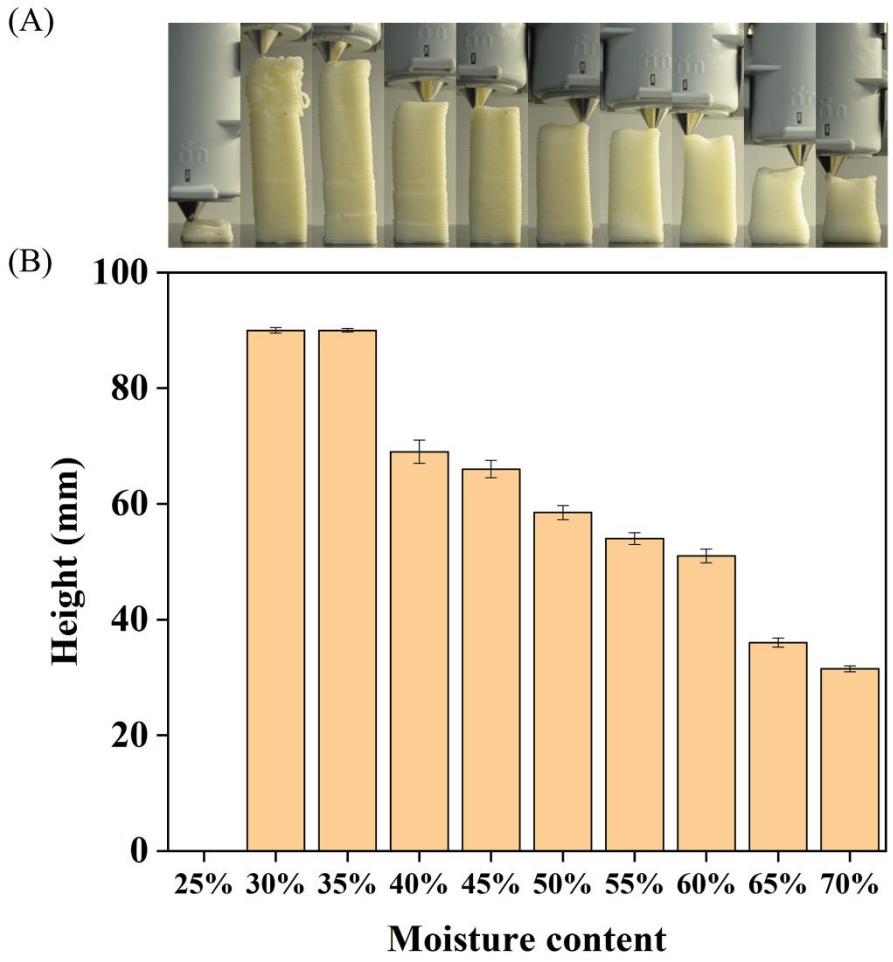

Fig. 4. 3D printing of hollow square column using PY with different moisture content (A) and the maximum height (B) that can be reached before collapse of the column.

3.3 Optimization of the pigment content

Since the pigment content would significantly affect the color saturation of the printing material, the dependence of saturation (S value) of the PPP-PY mixture (PPY) on PPP content was shown in Fig. 5. It was found the S value of the mixture increased from 7.6 to 66.2 with the PPP content increasing from 0.5 to 6 mg/100g. It may be noted that the slope of the curve gradually levels off. When the PPP content exceeded 5 mg/100 g, the S curve achieves an asymptotic maximum which indicated that further

increase of PPP content did not significantly improve the color saturation of the mixture. Therefore, the appropriate content of PPP was selected as 5 mg/100g.

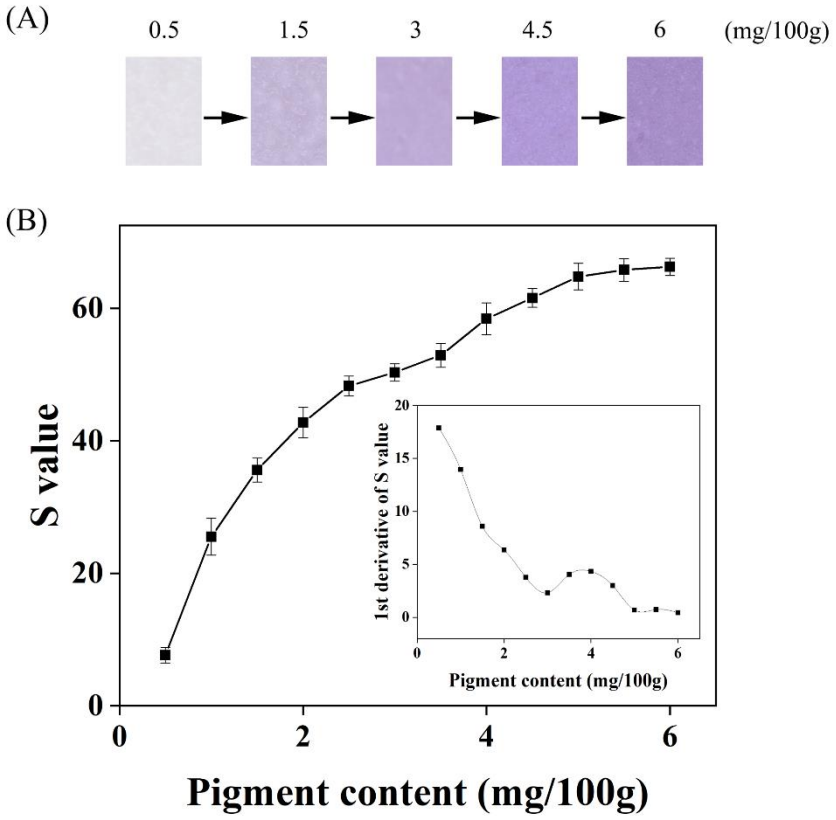

Fig. 5. Color change of PPY with different amounts of PPP (A), the S value of PPY under different PPP addition amount (B) and the curve of the 1st derivative of the S value curve (illustration).

3.4 Color control of the extruded line

3.4.1 Depending of PPY color on pH

The basic idea was to produce H^+ or OH^- through electrolysis, which would result in pH change of PY and consequently induce color change of PPY. Therefore, PPY with different pH was prepared to extract their corresponding color information (H value, part of images were shown in Fig. 6A). The relationship between the pH and H value

of PPY was shown in Fig. 6B, indicating that the H value of PPY gradually decreased with the increase of pH. With the increase of pH, the color of PPY changed from rose red (pH 0.32), pink (pH 6.7), green (pH 8.2) to yellow (pH 11.0). It should be mentioned that the change of H slowed down when too strong acidity or alkalinity formed indicating that the anthocyanins had basically been converted into flavonoid cations or chalcone [40]. The Boltzmann method was used to fit the relationship between pH and H value with a correlation coefficient (R^2) of 0.995, the fitting curve is as follows [41],

$$H\ value = -0.24342 + 1.16703/(1 + \exp((pH - 9.67704)/2.07802)\ ) \quad (1)$$

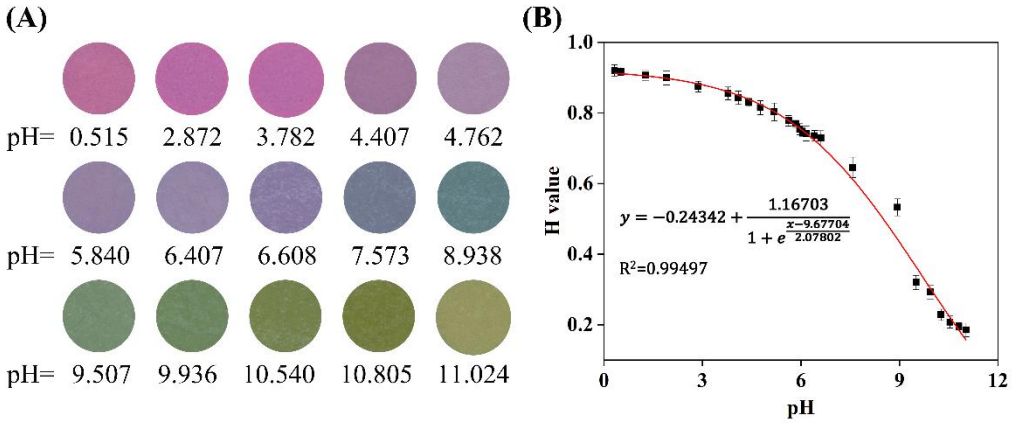

Fig. 6. Images of PPY at different pH (A) and the corresponding H value curve (B).

3.4.2 Depending of the extruded line color on the electrode potential

The colors of PPY samples extruded at a range of electrolytic potentials (-60 to 60 V with step of 5 V) were collected and are presented in Fig. 7A. When positive potential was applied, the color of extruded lines gradually turned from light purple to green, then darkened to yellow as the potential increased. When the applied potential was set to negative, the color changed from light purple to magenta, then to red.

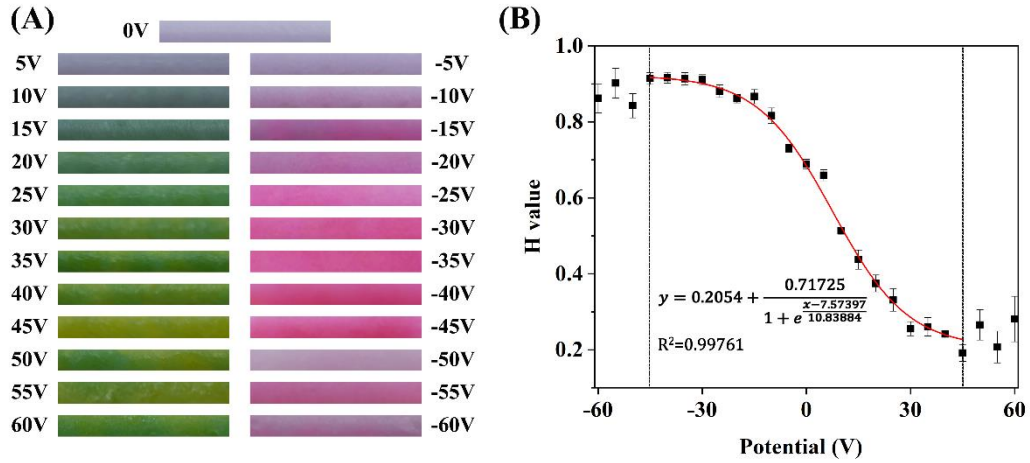

Fig. 7. Images of the extruded line at electrolytic potentials between -60 to 60 V (A) and the corresponding H value curve (B)

The H value of the extruded lines under different potential are shown in Fig. 7B, identifying the range from 0.192 to 0.916. It was found that the H value presented an S-shaped or sigmoidal trend, with slow change from -45 to -15 V and 30 to 45 V. The H value exhibited a marked reduction when increasing in the range -15 to 30 V, showing a correspondence with the color changes shown in Fig. 7A. Boltzmann method was used to fit the relationship between applied potential and H value (shown in Fig. 7B) with R^2 of 0.998 and the fitting curve is as following,

$$H \text{ value} = 0.2054 + 0.71725/\big(1 + \exp\big((E - 7.57397)/10.83884\big)\big) \quad (2)$$

$$(-45 \text{ v} < E < 45 \text{ v} \quad R^2 = 0.998)$$

3.4.3 Theoretical analysis of the electrolysis process

In principle, the variation in color achieved in the extruded lines was produced due to the formation of different acid-base environments in the hydrolysis reaction [42]. The following formula describes the associated chemical reaction [43]:

$$2H_2O \rightarrow 2H_2 + O_2 \quad (3)$$

The half reactions occurring on the cathode and anode, respectively, can be written as

$$\text{Cathode: } 2H_2O + 2e^- \rightarrow 2OH^- + H_2 \quad (4)$$

$$\text{Anode: } 2H_2O - 4e^- \rightarrow 4H^+ + O_2 \quad (5)$$

When a negative potential was applied, the nozzle acted as anode and the waste channel served as cathode, hydrogen ions thus accumulated based on Eq. (5), thereby realizing a strong acid environment and red color. On the contrary, gray-green, green or even yellow lines were produced when the nozzle worked as cathode due to the formation of an alkaline environment. However, if the potential was too high, appreciable electrolysis of water would occur generating a large amount of hydrogen or oxygen forming a significant and fluctuating gas [44], [45], [46]. This explains to variation in color at high potential. When the applied potential was between -40 to 30 V, the final pH of the extruded material depended on the applied potential level based on the following electrochemical theory [47].

Briefly, ionic substances diffused and migrated due to the existence of a concentration and potential gradient, which generates a current in the electrolyte [48]. The material balance of ionic category i may be described as in Eq. (6) [49]:

$$(\partial c_i)/\partial t + \nabla \cdot N_i = R_i \quad (6)$$

Where c_i is the concentration of the ionic species i (mol/m^3), R_i is the production term (mol/(m^3·s)) and N_i is the molar flux of the species i.

The current density J on the electrode surface can be expressed as Eq. (7) by Tafel laws [44], [50].

$$J = 10\text{^}((\eta - a)/b) \quad (7)$$

Where both a and b are constants. Considering these reactions and the current density in the electrolytic cell, the system can be expressed as a potential-based model [51]. The η (overpotentials) can be expressed as

$$\eta = E + E_{eq} \quad (8)$$

Where E is the electrode potential, E_{eq} is the equilibrium potential. In the experiment, the E was much larger than E_{eq}, so it is reasonable to approximate η as E.

As a rate quantity, current (I) was expressed by the following equation:

$$I = Q/t = J \cdot A \quad (9)$$

Where Q is the amount of charge flowing in time t, equal to the number of hydrogen ions and hydroxide radicals produced in the electrolysis process according to the law of conservation of charge, A is the available surface area for the reaction.

During the color 3D printing process, the nozzle diameter remained unchanged, resulting in a constant value of the electrolysis cross-section area (A). In addition, the same extrusion rate (v) was always maintained, and each extruded line segment had the same electrolysis time (t).

According to the Eq. (9), $\mathrm{Q} = \mathrm{J} \cdot \mathrm{A} \cdot \mathrm{t}$, substituting Eq. (7) and (8), the total charge produced by the electrolysis process in time t can be given as:

$$Q = 10\text{^}((E-a)/b)\ A \cdot t \qquad (10)$$

The concentration of hydrogen ions or hydroxide ions produced per unit time in the extrusion process can be obtained as in Eq. (11):

$$C_{H^+ \, or \, OH^-} = Q/(v \cdot t) = 10\text{^}((E-a)/b)\ A/v \qquad (11)$$

Therefore, the relationship between the applied potential and the pH of the extrusion line can be obtained as:

$$pH = -\log C_{H^+} = (a-E)/b - \log A + \log v \qquad (E < 0) \qquad (12)$$

$$pH = 14 - (-\log C_{OH^-}) = 14 - (a-E)/b + \log A - \log v \qquad (E>0) \quad (13)$$

Eq. (12) and Eq. (13) indicate that the pH of the extruded line is linearly related to the applied potential.

To verify this linear relationship, the pH values of the lines extruded at different potential were acquired according to Eq. (1), and ploted in Fig. 8 with potential as xaxis. It was found that the pH of the extruded line showed a good linear relationship with the applied potential from -40 to 30 V with R^2 of 0.986, which agreed well with Eq. (12) and Eq. (13). The above results and analysis suggested that the color of PPY could be conveniently controlled by adjusting the electrode potential.

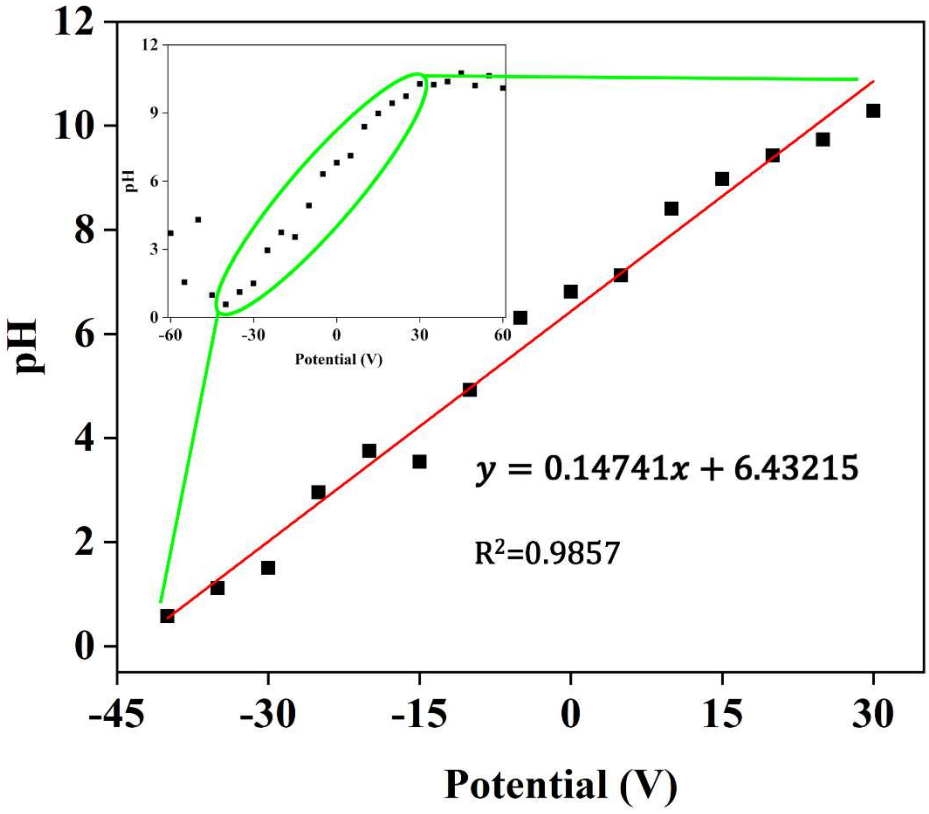

Fig. 8. The relationship between the electrolytic potential and the pH of the extruded line.

3.5 Color 3D printing of PY

In general, the color information (H value) in a printing file is extracted according to the present position of the nozzle, converted into the desired potential through the quantitative relationship between the electrode potential and the line color (Eq. (2)), then the programmable DC power supply is set to the desired potential to realize the pH and color.

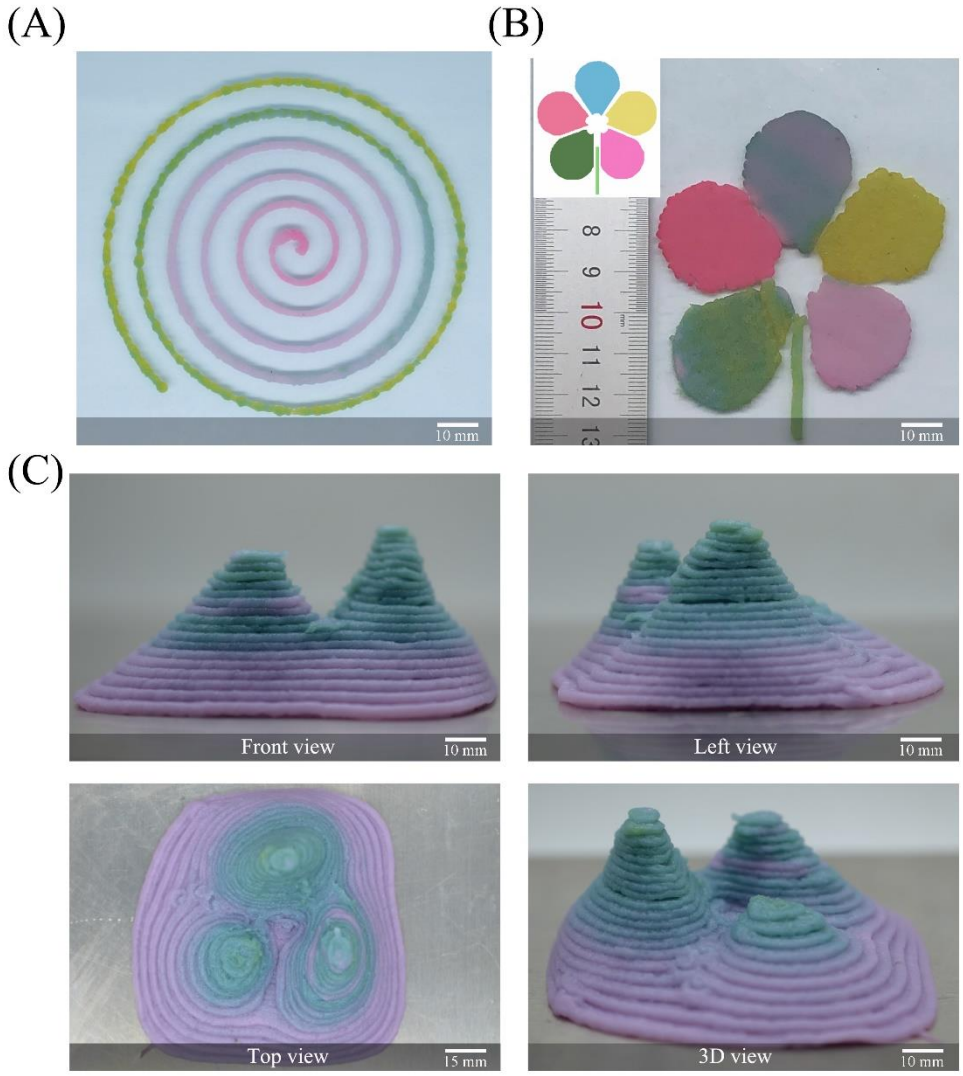

Fig. 9. A selection of color 3D printing works: the Archimedes spiral with gradient colors (A), the model and renderings of petals in six different colors (B), and the mountain-shaped sand table whose color changed with height (C).

Patterns of different dimensions were printed to demonstrate 3D color printing of food. As shown in Fig. 9A, an Archimedes spiral was printed to exhibit the continuous color-changing capacity (Supplementary Video 1), which shows graduated color of rose, magenta, purple, green, and yellow. The applied potential was set from -35 to 35 V according to the distance of the nozzle to the spiral center. A petal model with six colors

(purple, yellow, blue gray, red, dark green, light green) and the printed result is shown in Fig. 9B. A mountain-shaped sand table as shown in Fig. 9C was also printed. To express the height of the mountain, the range of electrode potential (0-25 V) was set according to the height of the model, purple was used for the base, green for the top and graduated colors in between with an increasing elevation. The printed models confirmed that the proposed method and device were capable of color 3D printing.

4. Conclusion

This study provided a novel approach for color 3D printing of food products, which explored the color-changing characteristics of natural pH sensitive pigments using an electrolysis method. Pulped Yam was used as a feedstock and pH sensitive pigments were extracted from purple potato which presented a wide hue range compared with other pigments. Process parameters were optimized as moisture content of 35% and PPP content of 5 mg/100g. Both theoretical derivation and experimental tests indicated that the pH of the extruded line was linearly related with the applied electrode potential, which could provide a hue range of 0.192-0.916 by conveniently adjusting the potential from -45 to 45 V. Color models of different dimensions were printed to demonstrate the practicality of the proposed method which exhibited acceptable results. Results suggest that the proposed method shows a promising potential in color 3D printing with the advantages of low cost, convenient control and simple structure. In future work, other pigments and more sources of feedstocks should be explored to provide enhanced color control capacity.

Acknowledgments

The authors gratefully acknowledge the financial support provided by National Key R&D Program of China (2018YFD0400803), National Natural Science Foundation of China (31801631), China Postdoctoral Science Foundation (2020M683372), National Natural Science Foundation of Jiangsu (BK20180865), and

Project of Faculty of Agricultural Equipment of Jiangsu University.

References

[1] M. Quanjin, M.R.M. Rejab, M.S. Idris, N.M. Kumar, M.H. Abdullah, G.R. Reddy, Recent 3D and 4D intelligent printing technologies: A comparative review and future perspective, Procedia Computer Science 167 (2020) 1210-1219.

[2] T. Webbe Kerekes, H. Lim, W.Y. Joe, G.J. Yun, Characterization of process–deformation/damage property relationship of fused deposition modeling (FDM) 3D-printed specimens, Additive Manufacturing 25 (2019) 532-544.

[3] S. Mantihal, R. Kobun, B.-B. Lee, 3D food printing of as the new way of preparing food: A review, International Journal of Gastronomy and Food Science 22 (2020) 100260.

[4] S. Holland, T. Foster, W. MacNaughtan, C. Tuck, Design and characterisation of food grade powders and inks for microstructure control using 3D printing, Journal of Food Engineering 220 (2018) 12-19.

[5] Y. Liu, D. Liu, G. Wei, Y. Ma, B. Bhandari, P. Zhou, 3D printed milk protein food simulant: Improving the printing performance of milk protein concentration by incorporating whey protein isolate, Innovative Food Science & Emerging Technologies 49 (2018) 116-126.

[6] F. Yang, M. Zhang, B. Bhandari, Y. Liu, Investigation on lemon juice gel as food material for 3D printing and optimization of printing parameters, LWT 87 (2018) 67-76.

[7] Y.-L. Cheng, C.-H. Chang, C.J.R.P.J. Kuo, Experimental study on leveling mechanism for material-jetting-type color 3D printing, (2020).

[8] J. Yuan, M. Zhu, B. Xu, G.J.R.P.J. Chen, Review on processes and color quality evaluation of color 3D printing, (2018).

[9] D. Ibrahim, T.L. Broilo, C. Heitz, M.G. de Oliveira, H.W. de Oliveira, S.M.W. Nobre, J.H.G. dos Santos Filho, D.N. Silva, Dimensional error of selective laser sintering, three-dimensional printing and PolyJet™ models in the reproduction of mandibular anatomy, Journal of Cranio-Maxillofacial Surgery 37(3) (2009) 167-173.

[10] V. Babaei, K. Vidimče, M. Foshey, A. Kaspar, P. Didyk, W.J.A.T.o.G. Matusik, Color contoning for 3D printing, 36(4) (2017) 1-15.

[11] H. Takahashi, P. Punpongsanon, J. Kim, Programmable Filament: Printed Filaments for Multi-material 3D Printing, Proceedings of the 33rd Annual ACM Symposium on User Interface Software and Technology, Association for Computing Machinery, Virtual Event, USA, 2020, pp. 1209–1221.

[12] M.A. Skylar-Scott, J. Mueller, C.W. Visser, J.A. Lewis, Voxelated soft matter via multimaterial multinozzle 3D printing, Nature 575(7782) (2019) 330-335.

[13] S.R. Mogali, W.Y. Yeong, H.K.J. Tan, G.J.S. Tan, P.H. Abrahams, N. Zary, N. Low-Beer, M.A. Ferenczi, Evaluation by medical students of the educational value of multi-material and multi-colored three-dimensional printed models of the upper limb for anatomical education, 11(1) (2018) 54-64.

[14] J. Vasquez, H. Twigg-Smith, J.T. O'Leary, N. Peek, Jubilee: An Extensible Machine for Multi-tool Fabrication, Proceedings of the 2020 CHI Conference on Human Factors in Computing Systems,

Association for Computing Machinery, Honolulu, HI, USA, 2020, pp. 1–13.
[15] M. Andó, M. Birosz, S. Jeganmohan, Surface bonding of additive manufactured parts from multi-colored PLA materials, Measurement 169 (2021) 108583.
[16] X. Zhai, X. Zou, J. Shi, X. Huang, Z. Sun, Z. Li, Y. Sun, Y. Li, X. Wang, M. Holmes, Y. Gong, M. Povey, J. Xiao, Amine-responsive bilayer films with improved illumination stability and electrochemical writing property for visual monitoring of meat spoilage, Sensors and Actuators B: Chemical 302 (2020) 127130.
[17] A. Castañeda-Ovando, M.d.L. Pacheco-Hernández, M.E. Páez-Hernández, J.A. Rodríguez, C.A. Galán-Vidal, Chemical studies of anthocyanins: A review, Food Chemistry 113(4) (2009) 859-871.
[18] F.J. Francis, P.C.J.C.R.i.F.S. Markakis, Nutrition, Food colorants: anthocyanins, 28(4) (1989) 273-314.
[19] J. Zhang, X. Zou, X. Zhai, X. Huang, C. Jiang, M. Holmes, Preparation of an intelligent pH film based on biodegradable polymers and roselle anthocyanins for monitoring pork freshness, Food Chemistry 272 (2019) 306-312.
[20] P. Bridle, C.F. Timberlake, Anthocyanins as natural food colours—selected aspects, Food Chemistry 58(1) (1997) 103-109.
[21] M.M. Giusti, R.E. Wrolstad, Acylated anthocyanins from edible sources and their applications in food systems, Biochemical Engineering Journal 14(3) (2003) 217-225.
[22] H.E. Khoo, A. Azlan, S.T. Tang, S.M.J.F. Lim, n. research, Anthocyanidins and anthocyanins: colored pigments as food, pharmaceutical ingredients, and the potential health benefits, 61(1) (2017) 1361779.
[23] L.J. Hendricks, J.T. Williams, Demonstration of electrochemical cell properties by a simple, colorful oxidation-reduction experiment, Journal of Chemical Education 59(7) (1982) 586.
[24] T.S. Kuntzleman, Electrochemistry with Simple Materials to Create Designs and Write Messages, Journal of Chemical Education 96(6) (2019) 1178-1181.
[25] A. Fogde, B. Kurtén, T. Sandberg, T.-P. Huynh, Colorimetric Hydrogel from Natural Indicators: A Tool for Electrochemistry Education, Journal of Chemical Education (2020).
[26] R.E. Zhou, How to Offer the Optimal Demonstration of the Electrolysis of Water, Journal of Chemical Education 73(8) (1996) 786.
[27] K. Yan, Y. Xiong, S. Wu, W.E. Bentley, H. Deng, Y. Du, G.F. Payne, X.-W. Shi, Electro-molecular Assembly: Electrical Writing of Information into an Erasable Polysaccharide Medium, ACS Applied Materials & Interfaces 8(30) (2016) 19780-19786.
[28] X. Zhai, Z. Li, J. Zhang, J. Shi, X. Zou, X. Huang, D. Zhang, Y. Sun, Z. Yang, M. Holmes, Y. Gong, M. Povey, Natural Biomaterial-Based Edible and pH-Sensitive Films Combined with Electrochemical Writing for Intelligent Food Packaging, Journal of Agricultural and Food Chemistry 66(48) (2018) 12836-12846.
[29] S. Chen, M. Wu, P. Lu, L. Gao, S. Yan, S. Wang, Development of pH indicator and antimicrobial cellulose nanofibre packaging film based on purple sweet potato anthocyanin and oregano essential oil, International Journal of Biological Macromolecules 149 (2020) 271-280.
[30] Z. Liu, M. Zhang, B. Bhandari, C. Yang, Impact of rheological properties of mashed potatoes on 3D printing, Journal of Food Engineering 220 (2018) 76-82.
[31] S. Zhu, M.A. Stieger, A.J. van der Goot, M.A.I. Schutyser, Extrusion-based 3D printing of food

445 pastes: Correlating rheological properties with printing behaviour, Innovative Food Science &
446 Emerging Technologies 58 (2019).
447 [32] I. Choi, J.Y. Lee, M. Lacroix, J. Han, Intelligent pH indicator film composed of agar/potato starch
448 and anthocyanin extracts from purple sweet potato, Food Chemistry 218 (2017) 122-128.
449 [33] R.E. Wrolstad, R.W. Durst, J. Lee, Tracking color and pigment changes in anthocyanin products,
450 Trends in Food Science & Technology 16(9) (2005) 423-428.
451 [34] M. Lanaro, D.P. Forrestal, S. Scheurer, D.J. Slinger, S. Liao, S.K. Powell, M.A. Woodruff, 3D
452 printing complex chocolate objects: Platform design, optimization and evaluation, Journal of Food
453 Engineering 215 (2017) 13-22.
454 [35] L. Gorjan, C. Galusca, M. Sami, T. Sebastian, F. Clemens, Effect of stearic acid on rheological
455 properties and printability of ethylene vinyl acetate based feedstocks for fused filament fabrication of
456 alumina, Additive Manufacturing 36 (2020) 101391.
457 [36] E.-J. Courtial, C. Perrinet, A. Colly, D. Mariot, J.-M. Frances, R. Fulchiron, C. Marquette, Silicone
458 rheological behavior modification for 3D printing: Evaluation of yield stress impact on printed object
459 properties, Additive Manufacturing 28 (2019) 50-57.
460 [37] D.-S. Sun, B. Yoo, Rheological and thermal properties of blend systems of rice flour and potato
461 starch, Food Science and Biotechnology 20(6) (2011) 1679-1684.
462 [38] S.K. Romberg, M.A. Islam, C.J. Hershey, M. DeVinney, C.E. Duty, V. Kunc, B.G. Compton,
463 Linking thermoset ink rheology to the stability of 3D-printed structures, Additive Manufacturing 37
464 (2021) 101621.
465 [39] Y. Wu, M. Niu, H. Xu, Pasting behaviors, gel rheological properties, and freeze-thaw stability of
466 rice flour and starch modified by green tea polyphenols, LWT 118 (2020) 108796.
467 [40] K. Halász, L. Csóka, Black chokeberry (Aronia melanocarpa) pomace extract immobilized in
468 chitosan for colorimetric pH indicator film application, Food Packaging and Shelf Life 16 (2018) 185-
469 193.
470 [41] B. Janssen, S. Pillen, N. Voet, A. Heerschap, B. Van Engelen, N. van Alfen, Quantitative muscle
471 ultrasound versus quantitative MRI in facioscapulohumeral dystrophy, Muscle & Nerve 50 (2014).
472 [42] S.A. Grigoriev, V.N. Fateev, D.G. Bessarabov, P. Millet, Current status, research trends, and
473 challenges in water electrolysis science and technology, International Journal of Hydrogen Energy
474 45(49) (2020) 26036-26058.
475 [43] F.e. Chakik, M. Kaddami, M. Mikou, Effect of operating parameters on hydrogen production by
476 electrolysis of water, International Journal of Hydrogen Energy 42(40) (2017) 25550-25557.
477 [44] M. Wang, Z. Wang, X. Gong, Z. Guo, The intensification technologies to water electrolysis for
478 hydrogen production – A review, Renewable and Sustainable Energy Reviews 29 (2014) 573-588.
479 [45] Q. Lei, B. Wang, P. Wang, S. Liu, Hydrogen generation with acid/alkaline amphoteric water
480 electrolysis, Journal of Energy Chemistry 38 (2019) 162-169.
481 [46] Y. Li, G. Yang, S. Yu, Z. Kang, J. Mo, B. Han, D.A. Talley, F.-Y. Zhang, In-situ investigation and
482 modeling of electrochemical reactions with simultaneous oxygen and hydrogen microbubble evolutions
483 in water electrolysis, International Journal of Hydrogen Energy 44(52) (2019) 28283-28293.
484 [47] J. Newman, K.E. Thomas-Alyea, Electrochemical systems, John Wiley & Sons2012.
485 [48] E. Nilsson, J. Berendson, E. Fontes, Electrochemical treatment of tumours: a simplified
486 mathematical model, Journal of Electroanalytical Chemistry 460(1) (1999) 88-99.

[49] E. Nilsson, Modelling of the electrochemial treatment of tumours, Kemiteknik, 2001.
[50] G.T. Burstein, A hundred years of Tafel's Equation: 1905–2005, Corrosion Science 47(12) (2005) 2858-2870.
[51] K. Zeng, D. Zhang, Recent progress in alkaline water electrolysis for hydrogen production and applications, Progress in Energy and Combustion Science 36(3) (2010) 307-326.